

Thermal and optical analysis of Te-substituted Sn–Sb–Se chalcogenide semiconductors

Ravi Chander · R. Thangaraj

Received: 12 August 2009 / Accepted: 5 November 2009 / Published online: 27 November 2009
© Springer-Verlag 2009

Abstract Bulk amorphous samples of Te-substituted $\text{Sn}_{10}\text{Sb}_{20}\text{Se}_{70-X}\text{Te}_X$ ($0 \leq X \leq 12$) were prepared using a melt quenching technique. Calorimetric studies of the samples were performed using differential scanning calorimetry (DSC) and the glass transition temperature and crystallization temperature were evaluated from DSC scans. The glass transition temperature T_g exhibits a sharp decrease for small Te substitution of $X = 2$, thereafter increases with increase in Te content up to $X = 10$, and then decreases for further Te substitution. The apparent activation energy for glass transition and the activation energy for crystallization were calculated using Kissinger, modified Kissinger, and Matusita equations. The change in glass transition temperature T_g has been explained based on the bond formation energy of different heteropolar bonds. The optical band gap of thermally evaporated thin films of $\text{Sn}_{10}\text{Sb}_{20}\text{Se}_{70-X}\text{Te}_X$ ($0 \leq X \leq 12$) was calculated from reflectance and transmittance data. The optical band gap variation with tellurium content exhibits a sharp decrease for an initial tellurium substitution of $X = 2$ similar to that of the glass transition temperature and thereafter a peak is observed in optical band gap around $X = 4$ composition.

1 Introduction

Chalcogenide materials are widely studied for their potential applications in active as well as passive solid-state electronic and optical devices. The applications include photoreceptors in xerography [1], optical and electronic memories

[2, 3], infrared (IR) optical fibers and waveguides [4], and non-linear optics [5]. Chalcogenide materials containing S, Se, and Te show high transmittance in the ranges 0.8–7, 1–10, and 2–12 μm , respectively [6] that makes them potential candidates for IR optical devices. Heavy atomic mass element doped chalcogenide materials exhibit a small glass forming region but have the advantage of higher transmittance in the IR region due to low optical losses [2]. This technological advantage increases interest in chalcogenide systems containing Sn and Sb as heavy elements. The effect of substitution or impurity addition on physical properties of these materials has been widely studied in chalcogenide materials. The most commonly studied substitutions or impurity additions are from group IV or group V elements, which are network formers and change the mean coordination number Z of chalcogenide material. The mean coordination number Z plays a crucial role in chalcogenide materials exhibiting two types of threshold at $Z = 2.4$ [7] and 2.67 [8], around which many physical properties of the materials show anomalous behavior. The aim of the present work is to study the effect of isoelectronic substitution of the chalcogen element Se with Te on thermal and optical properties of the glassy $\text{Sn}_{10}\text{Sb}_{20}\text{Se}_{70}$ system. The base composition is chosen in such a way to have a mean coordination number $Z = 2.4$ (rigidity percolation threshold) so as to study the effect of substitution of one chalcogen atom with another on physical properties of the material. There are reports on the Se–Te system having better corrosion resistance [9] that makes it a prospective material for phase-change memory application [10], which involves an amorphous–crystalline phase transformation. The crystallization kinetics of amorphous materials has been widely discussed in the literature [11–13]. Different techniques, viz. isothermal and non-isothermal, are employed to study the crystallization kinetics in amorphous solids. In the isothermal technique, the

R. Chander (✉) · R. Thangaraj
Semiconductor Laboratory, Department of Applied Physics, Guru Nanak Dev University, Amritsar 143005, India
e-mail: rcohri@yahoo.com

temperature is quickly increased to above the glass transition temperature (T_g) and the heat evolved is analyzed. On the other hand, in the case of non-isothermal technique, the sample is heated at a constant heating rate and the heat evolved is analyzed. The non-isothermal technique employs differential scanning calorimetry (DSC). There are many theoretical models which have been developed to explain the crystallization kinetics [14–17]. The apparent activation energy for glass transition and the activation energy for crystallization have been calculated using these models.

2 Experimental details

Bulk samples of $\text{Sn}_{10}\text{Sb}_{20}\text{Se}_{70-X}\text{Te}_X$ ($0 \leq X \leq 12$) were prepared using a conventional melt quenching technique. The details of bulk sample preparation are described elsewhere [18]. Thin films were deposited onto well-cleaned glass substrates by a thermal evaporation technique using as-prepared bulk samples as source material. The substrate cleaning steps involved acetone rinsing followed by piranha ($\text{H}_2\text{SO}_4 + \text{H}_2\text{O}_2$ in 2:1 ratio) cleaning and finally de-ionized water rinsing. The substrates were kept in acetone before placing into a vacuum chamber. The deposition was carried out using a coating unit (HIND HIVAC model no. 12A 4D) at $\sim 10^{-5}$ mbar pressure with current in the secondary coil $I_s = 50$ A and the thickness of the films was kept at ~ 1 μm . Thin films were kept in the vacuum chamber for ~ 24 h after deposition for attaining metastable equilibrium [19]. The as-prepared bulk material was ground finely into powder form and used for X-ray diffraction (XRD) and differential scanning calorimetry (DSC) studies. XRD was performed using a Phillips PAN ANALYTICAL machine with X-ray of the $\text{Cu } K_\alpha$ line in order to verify the amorphous nature of as-prepared samples. DSC scans were performed at different heating rates using a Mettler Toledo Star^e system in the temperature range from room temperature to 773 K under N_2 gas environment and an empty reference pan. The glass transition temperature evaluated from DSC scans is defined as the temperature corresponding to the intersection of two linear portions adjoining the transition elbow of the DSC trace in the endothermic direction. The onset of crystallization temperature T_c is defined as the temperature corresponding to the intersection of two linear portions adjoining the transition elbow of the DSC trace in the exothermic direction. The crystallized fraction X_c at a particular temperature T in the exothermic peak representing crystallization was calculated using the relation $X_c = A_T/A$. A in the relation is the total area of the exothermic peak and A_T is the area between the onset of crystallization temperature T_c and that particular temperature T . Transmittance and specular reflectance w.r.t. air were measured at room temperature using a UV-VIS-NIR spectrophotometer (VARIAN Cary 500) in the wavelength range 200–3000 nm with a slit width of 1 nm.

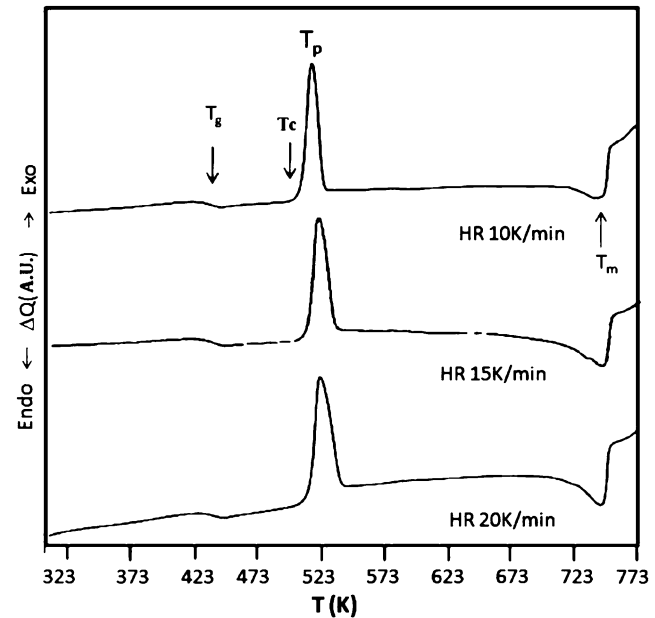


Fig. 1 DSC plot of $\text{Sn}_{10}\text{Sb}_{20}\text{Se}_{64}\text{Te}_6$ at different heating rates. Glass transition, peak crystallization, and melting temperatures are marked in the plot

3 Results and discussion

X-ray diffraction studies of as-prepared samples revealed the absence of any sharp peak that indicates the amorphous nature of these samples. Figure 1 shows the typical DSC plot of the sample $X = 6$ representing a single glass transition, a single crystallization, and a single melting peak. All samples with different tellurium contents showed similar plots. Thermal parameters evaluated from DSC scans are discussed in the following subsections.

3.1 Glass transition

The glass transition temperature T_g as obtained from the DSC plots shows a monotonic increase for tellurium substitution $X = 2$ to $X = 10$ and then it decreases for further substitution as shown in Fig. 2. The value of T_g shows a shift towards higher temperature with increase in heating rate, α , as shown in Fig. 3 for the $X = 2$ sample. The empirical relation for glass transition variation with heating rate holds good for all samples:

$$T_g = A + B \ln \alpha, \quad (1)$$

where A and B are constants. The value of the constant B ranges from 2.35 to 3.60 that reveals the structural changes occurring in the sample, as the composition is varied [20]. The apparent activation energy for glass transition was calculated using the Kissinger equation [21]

$$\ln\left(\frac{T_g^2}{\alpha}\right) + \text{constant} = E_{\text{gl}}/RT_g, \quad (2)$$

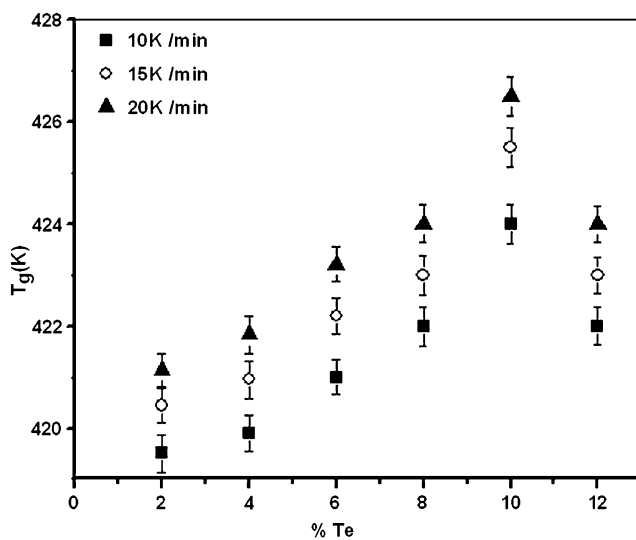


Fig. 2 Variation of T_g with tellurium content in the samples

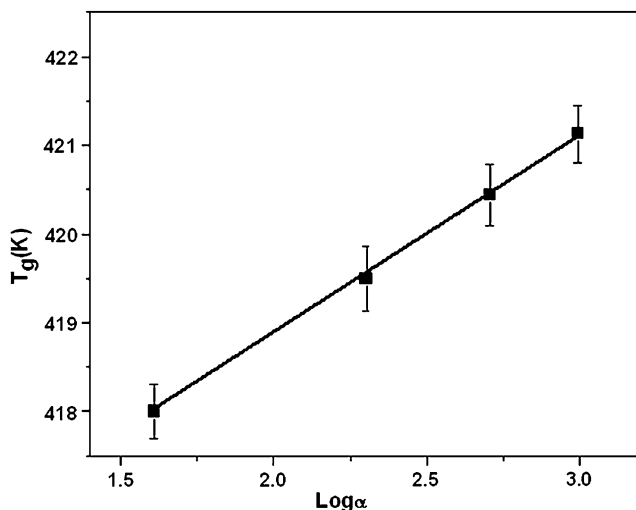


Fig. 3 Plot of linear variation of T_g with heating rate α for $\text{Sn}_{10}\text{Sb}_{20}\text{Se}_{68}\text{Te}_2$ sample

where α , R , and E_{gl} are the heating rate, gas constant, and apparent activation energy for glass transition, respectively. The slope of the $\ln(T_g^2/\alpha)$ versus $1000/T_g$ plot gives the value of E_{gl} as shown in Fig. 4. The apparent activation energy for glass transition shows a decreasing trend with increasing tellurium content.

3.2 Crystallization

The activation energy for crystallization was calculated using the modified Kissinger equation [14]

$$\ln(\alpha^n/T_p^2) = -mE_c/RT_p + \ln K, \quad (3)$$

where K is a constant that contains a factor representing the thermal history of the sample. The factors n and m have val-

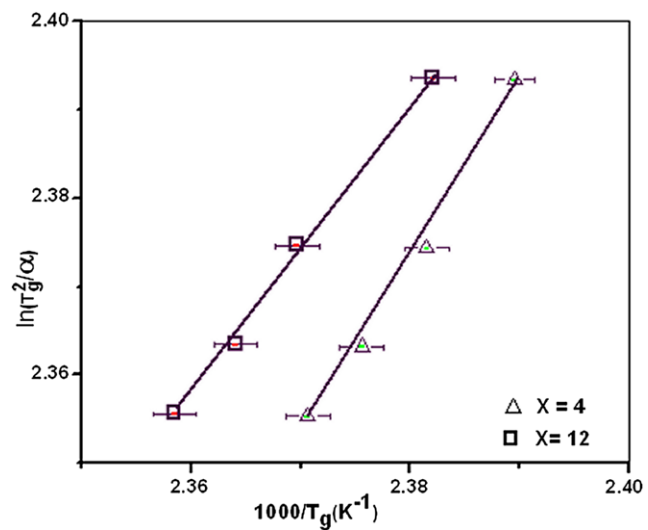


Fig. 4 Plot of $\ln(T_g^2/\alpha)$ versus $1000/T_g$ for samples $\text{Sn}_{10}\text{Sb}_{20}\text{Se}_{70-X}\text{Te}_X$ with $X = 4$ and 12

ues 1–4 depending upon the morphology of the growth. Figure 5 shows a plot of $\ln\alpha$ versus $1000/T_p$; the slope of the plot gives the value of mE_c/n . In the case of non-isothermal crystallization, the activation energy can also be calculated using the Matusita equation [15]

$$\ln\{-\ln(1-X_c)\} = -n\ln\alpha - 1.052mE_c/RT_p, \quad (4)$$

where X_c is the volume fraction of crystals precipitated in the glass upon heating at a uniform heating rate, α , E_c is the crystallization activation energy, T_p is the peak crystallization temperature, and n and m are constants representing the morphology of the growth. Mahadevan et al. [16] have shown that n can take values 1–4, depending upon different glass–crystal transformation mechanisms. $n = 4$ represents volume nucleation and three-dimensional growth, $n = 3$ represents volume nucleation and two-dimensional growth, $n = 2$ represents volume nucleation and one-dimensional growth, $n = 1$ represents surface nucleation and one-dimensional growth from the surface to inside. The value of n can be calculated from the slope of the straight line of the plot of $\ln[-\ln(1-X_c)]$ versus $\ln\alpha$ at constant temperature. Figure 6 shows the plot of $\ln[-\ln(1-X_c)]$ versus $\ln\alpha$ at two different temperatures for the $X = 6$ sample. The value of n calculated from the plot ranges between 4.15 and 4.51. Since the samples were not given any prior heat treatment before DSC experiments, the value of m can be taken as $n - 1$, i.e. 3. Thus, in the case of our samples, the values of $n = 4$ and $m = 3$ reveal volume nucleation and three-dimensional growth. Figure 7 shows the plot of $\ln[-\ln(1-X_c)]$ with $1000/T_p$ at different heating rates for the $X = 6$ sample. The slope of the straight line drawn in the plot gives the value of mE_c . The deviation from a straight line in the plot at higher temperature might be due to saturation of nucleation sites in the process of crystallization [22].

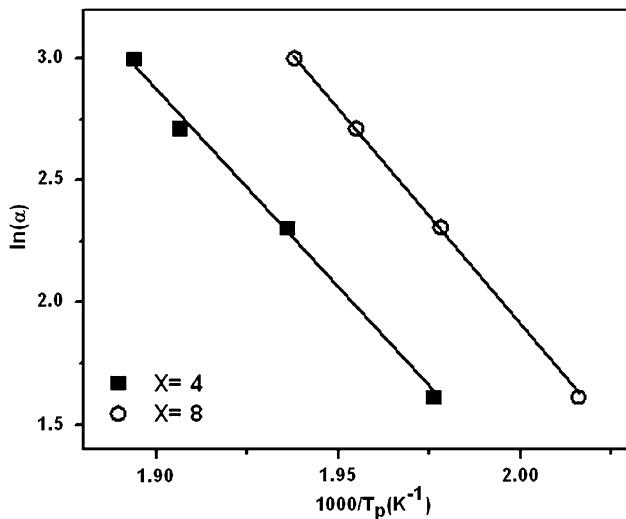


Fig. 5 Plot of $\ln \alpha$ with $1000/T_p$ for $X = 4$ and 8

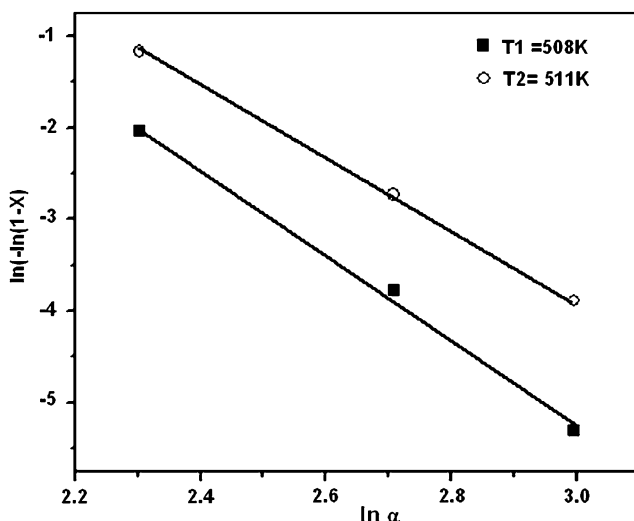


Fig. 6 Plot of $\ln[-\ln(1-X_c)]$ and $\ln \alpha$ at two different temperatures for $\text{Sn}_{10}\text{Sb}_{20}\text{Se}_{64}\text{Te}_6$ sample

Using the values of n and m , the activation energy of crystallization was calculated for both modified Kissinger and Matusita methods. The calculated values of E_c are given in Table 1 as E_c (MK) and E_c (ME) for the modified Kissinger equation and the Matusita equation, respectively.

3.3 Glass stability

Different simple quantitative methods have been suggested for evaluating stability of glasses [23–26] using parameters such as the glass transition temperature T_g , the onset of crystallization temperature T_c , the peak crystallization temperature T_p , and the melting temperature T_m obtained from DSC scans. The calculated values of glass stability parameters are given in Table 2. These parameters reflect that the $X = 4$

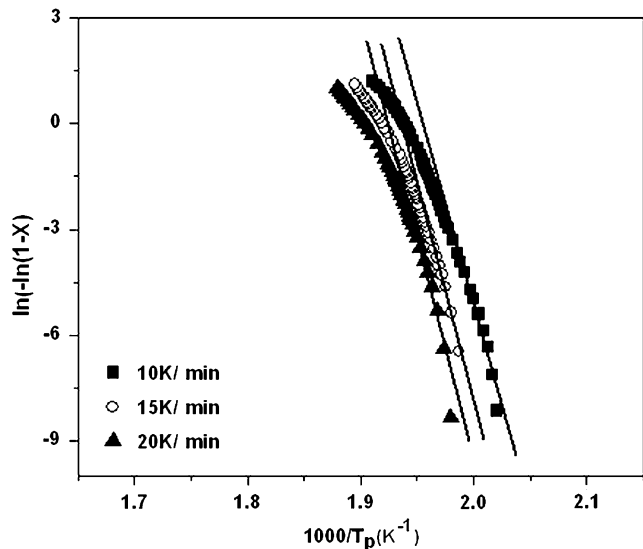


Fig. 7 Plot of $\ln[-\ln(1-X_c)]$ versus $1000/T_p$

sample shows the best glass stability with higher H_r and S values. The variation in glass transition temperature T_g can be explained on the basis of heteronuclear bond energies of different possible bonds formed in different compositions [18]. The sharp decrease in the glass transition temperature T_g from 426 K at $X = 0$ [18] on substitution of a small atomic % of tellurium might be due to formation of weaker homopolar Te–Te bonds (bond formation energy 259 kJ/mole). This is corroborated by the observed Te phase in the annealed sample of composition $X = 2$ [18]. Since the homopolar Te–Te bond is weakest among all possible bonds, this leads to a decrease in the glass transition temperature T_g . Further substitution of tellurium up to $X = 10$ increases the glass transition temperature T_g . This might be due to formation of heteropolar Sb–Te (bond energy 277.48 kJ/mole) and Sn–Te (bond energy 359.8 kJ/mole) bonds, which are relatively stronger than the Te–Te bond. This is supported by the fact that annealed samples with higher tellurium contents revealed Sb_2Te_3 phase and showed an increase in the value of d spacing of different planes of Sb_2Se_3 and SnSe_2 phases that might be related to tellurium substitution at the Se lattice position in these phases [18]. The decrease in T_g on further substitution of Te might be again formation of the weaker Te–Te bond due to abundance of Te in the $X = 12$ sample.

3.4 Optical properties

Figure 8 shows transmission spectra of thin-film samples in the wavelength range 500–2500 nm. The absorption coefficient α was calculated from transmission and reflection (not shown in Fig. 8) spectra using the relation

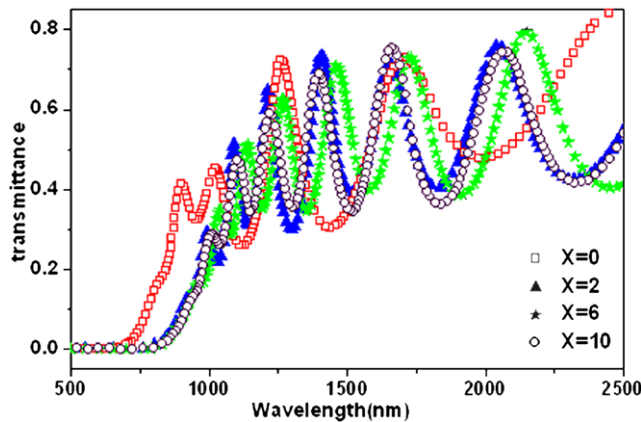
$$T = (1 - R)^2 \exp(-\alpha d). \quad (5)$$

Table 1 Values of B , E_{gl} , n , m , E_c (MK), and E_c (ME)

% Te	B	E_{gl} (Kcal mol $^{-1}$)	mE_c/n (MK) (Kcal mol $^{-1}$)	n	m	E_c (MK) (Kcal mol $^{-1}$)	mE_c (ME) (Kcal mol $^{-1}$)	E_c (ME) (Kcal mol $^{-1}$)
2	2.35	73.81	20.53	4.31	3	29.50	88.65	29.55
4	2.51	71.29	20.01	4.51	3	30.08	129.5	43.16
6	3.20	56.37	21.19	4.23	3	29.87	107.22	35.74
8	3.00	60.44	17.54	4.28	3	25.02	121.95	40.65
10	3.60	50.74	18.83	4.15	3	26.04	115	38.33
12	3.00	61.77	20.74	4.33	3	29.93	106.5	35.5

Table 2 Various thermal stability parameters

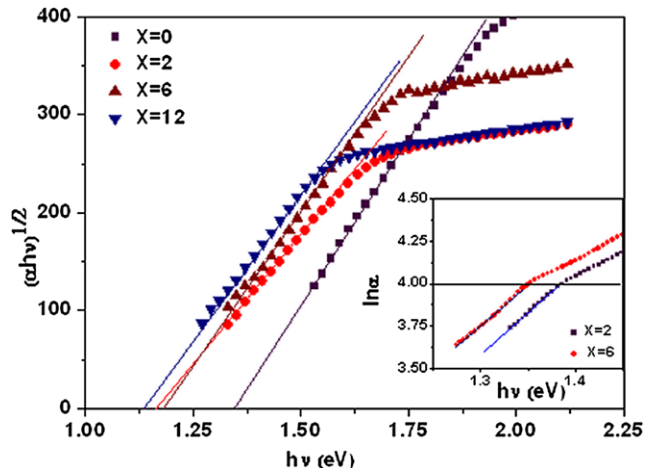
% Te	T_g	T_c	T_p	T_m	H_r	H'	S	T_{rg}
2	419.5	499	508	739	0.34416	0.18951	1.7056	0.56766
4	419.9	503	516.5	742	0.36851	0.1979	2.67171	0.5659
6	421	504.75	513.3	743	0.36461	0.19893	1.70086	0.56662
8	422	501.21	505.5	740	0.33778	0.1877	0.80524	0.57027
10	424	494.26	499.3	738	0.29434	0.16571	0.83517	0.57453
12	422	479	484	724	0.2375	0.13507	0.67536	0.58287

**Fig. 8** Plot of transmission spectra of thin films with $X = 0, 2, 6$, and 10

In amorphous chalcogenide materials, spectral variation of the absorption coefficient α exhibits three regions [27], viz. a weak absorption region where α is small of the order of unity, an exponential region that extends over four orders of magnitude, and a strong absorption region where α is $> 10^4 \text{ cm}^{-1}$ that represents inter-band transitions. The strong absorption region can be expressed by the relation [27]

$$\alpha h\nu = B(h\nu - E_g)^n, \quad (6)$$

where E_g is the optical band gap and B is a constant. The value of the exponent n determines the type of inter-band transition in a particular energy range. The value $n = 1$ rep-

**Fig. 9** Plot of $(\alpha h\nu)^{1/2}$ versus $h\nu$ for optical band gap. Inset is plot of $\ln \alpha$ versus $h\nu$

resents a direct allowed transition, $n = 2$ represents an indirect allowed transition, while $n = 3/2$ represents a direct forbidden transition. Chalcogenide amorphous semiconductors generally exhibit an indirect allowed transition with $n = 2$. Figure 9 shows the plot of $(\alpha h\nu)^{1/2}$ versus $h\nu$ for different compositions. The band gap E_g and constant B can be obtained from extrapolation of the linear region of the plot up to zero absorption and the slope of that linear region, respectively, as shown in Fig. 9.

The absorption coefficient in the energy range below the optical band gap is expressed in exponential form as $\alpha = \alpha_0 \exp(h\nu/E_u)$, where E_u represents the Urbach energy

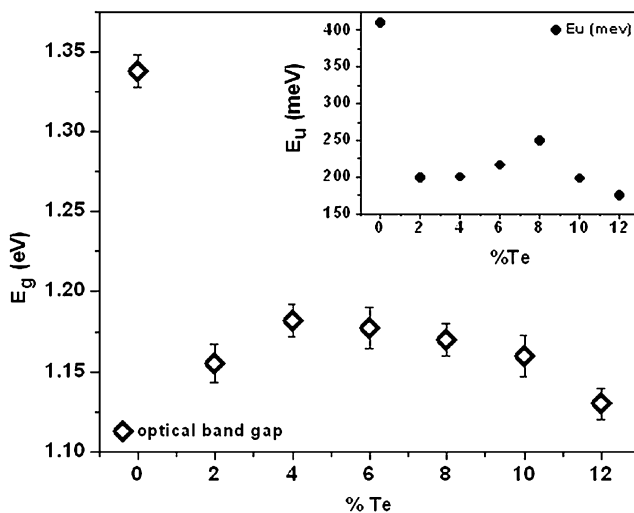


Fig. 10 Plot showing variation of optical band gap with tellurium content. Inset shows variation of urbach energy with tellurium content

that is interpreted as the width of localized states adjoining band edges due to disorder in the amorphous material. Thus, exponential dependence of the absorption coefficient dominates with optical transitions from localized states adjoining the valence band and the conduction band. The value of the Urbach energy is obtained from the slope of a straight-line portion of the plot between $\ln \alpha$ and $h\nu$ as shown in the inset of Fig. 9 for $X = 2$ and 6. Figure 10 shows the variation of the optical band gap E_g with tellurium content that represents a sharp decrease in band gap for initial tellurium content similar to that of the glass transition temperature T_g , which slightly increases for higher tellurium content up to $x = 4$ and then slowly decreases afterwards. The trends can be explained with the help of bond formation energy [18] and the model given by Kastner [28]. The decrease in the band gap E_g with Te substitution might be due to two factors, the first being the interaction of lone-pair electrons of Te, which broadens into a band just above the lone-pair band of Se as reflected from ionization energy levels of the elements Te and Se [28]. Thus, the lone-pair band of Te governs the top of the valence band and leads to narrowing of the band gap in all the compositions containing tellurium. The second factor related to the steep decrease in the band gap E_g for the $X = 2$ composition might be due to the fact that this composition contains Te–Te weakest bonds [18] that shift down the anti-bonding band (conduction band) of the material and further narrow down the band gap [28]. The slight increase of the optical band gap from $X = 2$ to $X = 4$ might be due to the absence of Te–Te bonds in the $X = 4$ composition. The decrease in band gap is consistent with the observed decrease in the Urbach energy for Te-substituted compositions as shown in the inset of Fig. 10. The localized states adjoining valence and conduction bands are now being superimposed with the lone-pair band of Te

that decreases the width of localized states beyond the valence band as reflected in a decreased value of the Urbach energy.

4 Conclusions

A thermal investigation of the chalcogenide system $\text{Sn}_{10}\text{Sb}_{20}\text{Se}_{70-x}\text{Te}_x$ was carried out and thermal parameters like the glass transition temperature, crystallization temperature, etc., were evaluated from DSC plots. The glass transition temperature exhibits a steep decrease upto $X = 2$ followed by a monotonous increase upto $X = 10$ and then decreases. The variation is explained with the bond formation energy of different heteropolar and homopolar bonds possible in different compositions. The crystallization kinetics showed volume nucleation and three-dimensional growth of crystallites. Thermal stability parameters showed that the alloy with $X = 4$ has the best glass stability. The optical band gap and Urbach energy were calculated from transmission and reflection data. Optical band gap exhibits a steep decrease for initial substitution of tellurium upto $X = 2$ similar to that of glass transition temperature and thereafter a peak in optical band gap is observed around $X = 4$ composition.

Acknowledgements The authors want to thank Dr S. Sathiaraj of Botswana University for optical and EDAX measurements, RSIC, Punjab University Chandigarh for XRD experiments, and CIL, NIPER Mohali for their cooperation in conducting DSC runs. RC wants to acknowledge Dr Praveen Kumar for useful discussions.

References

1. A. Onozuka, O. Oda, J. Non-Cryst. Solids **103**, 289 (1988)
2. S.R. Elliot, *Physics of Amorphous Materials*, 2nd edn. (Longman, London, 1991)
3. S. Fugimori, S. Sagi, H. Yamzaki, N. Funakoski, J. Appl. Phys. **64**, 100 (1988)
4. T. Katsuyama, S. Satoh, H. Matsumura, J. Appl. Phys. **71**, 4132 (1992)
5. M. Asobe, Opt. Fiber Technol. **3**, 142 (1997)
6. J.S. Sanghera, I.D. Aggarwal, J. Non-Cryst. Solids **256–257**, 6 (1999)
7. J.C. Phillips, M.F. Thorpe, Solid State Commun. **53**, 699 (1985)
8. G. Lucovsky, F.L. Galeener, R.H. Geils, R.C. Keezer, *The Structure of Non-Crystalline Materials* (Taylor & Francis, London, 1977), p. 127
9. A.H. Moharram, A.A. Abu-sehly, M. Abu El-Oyoun, A.S. Soltan, Physica B **324**, 344 (2002)
10. M. Wuttig, N. Yamada, Nature Mater. **6**, 824 (2007)
11. E.R. Shaaban, M.T. Dessouky, A.M. Abousehly, J. Phys.: Condens. Matter **19**, 09212 (2007)
12. N. Afify, J. Non-Cryst. Solids **142**, 247 (1992)
13. A.S. Soltan, Physica B **307**, 78 (2001)
14. D.R. Macfarlane, M. Matecki, M. Poulain, J. Non-Cryst. Solids **64**, 351 (1984)
15. K. Matusita, T. Konatsu, R. Yokota, J. Mater. Sci. **19**, 291 (1984)

16. S. Mahadevan, A. Giridhar, A.K. Singh, J. Non-Cryst. Solids **88**, 11 (1986)
17. K. Matusita, S. Sakka, Phys. Chem. Glasses **20**, 81 (1979)
18. R. Chander, R. Thangaraj, Eur. Phys. J. Appl. Phys. **48**, 10302 (2009)
19. M. Abkowitz, Polym. Eng. Sci. **24**, 1149 (1984)
20. M. Lasocka, Mater. Sci. Eng. **23**, 173 (1976)
21. H.E. Kissinger, J. Res. Natl. Bur. Stand. **57**, 217 (1956)
22. J. Colemenero, J.M. Bandarian, J. Non-Cryst. Solids **30**, 263 (1978)
23. A. Dietzel, Glasstech Ber. **22**, 41 (1968)
24. A. Hruby, Czech J. Phys. B **22**, 1187 (1972)
25. M. Saad, M. Poulain, Mater. Sci. Forum **19–20**, 11 (1987)
26. S. Sakka, J.D. Mackenzie, J. Non-Cryst. Solids **6**, 145 (1971)
27. J. Tauc, *Amorphous and Liquid Semiconductors* (Plenum, New York, 1974), p. 172
28. M. Kastner, Phys. Rev. Lett. **28**, 355 (1972)